CHAPTER 7

Target Fluctuation Models

Mark A. Richards

Chapter Outline

7.1 INTRODUCTION

A sample of radar data is composed of either interference alone or interference plus target echoes. The interference is, at a minimum, receiver noise and might also include clutter echoes, electromagnetic interference (EMI) from other transmitting sources (e.g., radars, television stations, cellular telephones), and hostile jamming. Most of these interfering signals are noise-like and are therefore modeled as random processes. Occasionally, a target echo will also be present in a particular sample of radar data. One of the major tasks of a radar system is to detect the presence of these targets when they occur. As was seen in Chapter 3, this is generally accomplished by *threshold detection*.

Chapter 3 introduced the *nonfluctuating* target, that is, one in which the radar cross section (RCS) remains constant over the group of samples used for detection. While this is a useful reference point, it is rarely a realistic model of real-world radar targets. Chapter 6 described how target size, materials, shape, and viewing angle contribute to determining RCS. Variations in radar-target geometry, target vibration, and radar frequency changes can lead to variations in target RCS, resulting in *fluctuating targets*. In this chapter, common models for the statistics of target echoes are discussed, with an emphasis on the traditional Swerling models. The effect of these models on radar detection performance is considered in Chapter 15.

7.2 | RADAR CROSS SECTION OF SIMPLE TARGETS

7.2.1 Basic Scatterers

The simplest radar target is a perfectly conducting sphere, such as those shown in Figure 7-1. Because of its spherical symmetry, the RCS of a sphere is independent of aspect angle. As discussed in Chapter 6 it is not, however, independent of radar frequency. Figure 7-2 shows the normalized RCS of a sphere as a function of its size relative to the radar wavelength, computed using the Mies series solution in [1]. It oscillates dramatically when the sphere is relatively small compared with the radar wavelength λ but approaches an asymptotic value of πa^2 (where a is the radius of the sphere) when the sphere is large compared with the wavelength. Another example of a relatively simple target with a known RCS is a *corner reflector* such as the dihedral or trihedral shown in Figure 7-3. Corner

FIGURE 7-1 ■ Examples of RCS calibration spheres. (Courtesy of Professor Nadav Levanon, Tel-Aviv University.)

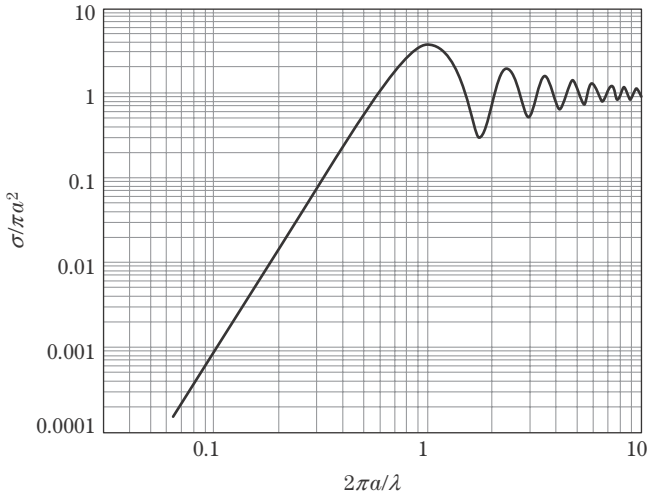

FIGURE 7-2 ■ Normalized RCS of a perfectly conducting sphere as a function of radius a and wavelength λ.

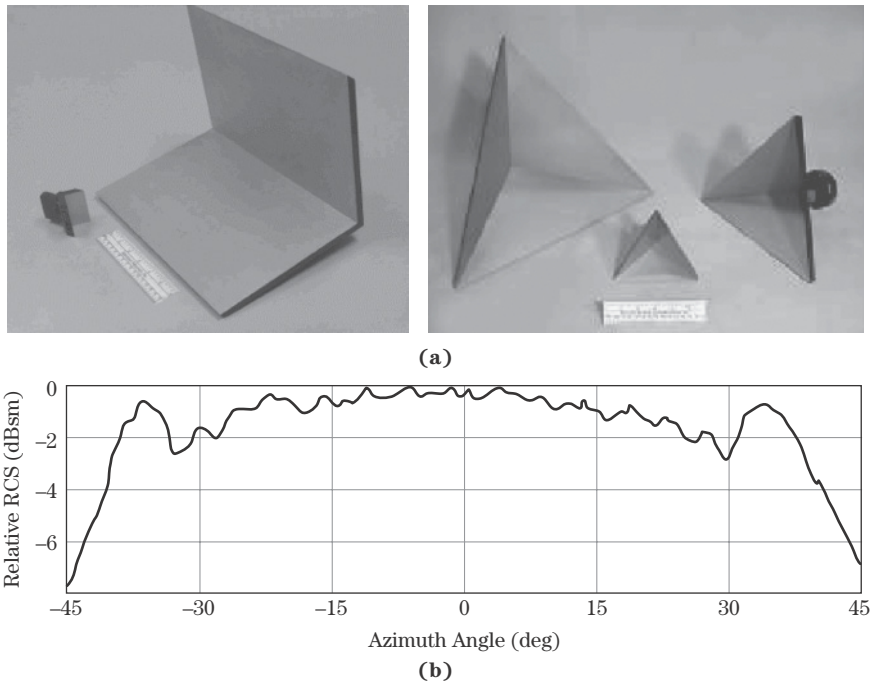

FIGURE 7-3 ■ Corner reflectors. (a) Dihedrals. (b) Trihedrals. (Courtesy of Professor Nadav Levanon, Tel-Aviv University.)

reflectors are meant to be illuminated along their axis of symmetry. For example, the RCS of a square-sided trihedral of dimension a on a side is $12\pi a^4/\lambda^2$ when viewed along the axis of symmetry [1]. The RCS of both corner reflectors (provided the radar aspect angle is near the axis of symmetry) and spherical targets can be characterized by a single value for a given wavelength and polarization. Thus, these simple targets have deterministic, not statistical, RCS models. Nonetheless, the radar received signal is the sum of these deterministic echoes and random interference and still requires a statistical characterization.

7.2.2 Aspect Angle and Frequency Dependence of RCS

The radar cross section of real targets cannot be effectively modeled as a simple constant. In general, RCS is a complex function of aspect angle, frequency, and polarization even for relatively simple targets. Furthermore, received power at the radar (target echo only, not including noise or other interference) is proportional to target RCS as seen in the radar range equation. Thus, RCS fluctuations result in received target power fluctuations.

A simple example of frequency and aspect dependence of the RCS of a "complex" target is the two-scatterer "dumbbell" target shown in Figure 7-4. If the nominal range, R, is much greater than the separation, D, the range to the two scatterers is approximately

$$R_{1,2} \approx R \pm \frac{D}{2}\sin\theta \tag{7.1}$$

If the transmitted signal is $ae^{j2\pi ft}$, the echo from each scatterer will be proportional to $ae^{j2\pi f(t-2R_{1,2}/c)}$. The voltage, $y(t)$, of the composite echo is therefore

$$\begin{aligned} y(t) &\propto ae^{j2\pi f(t-2R_1/c)} + ae^{j2\pi f(t-2R_2/c)} \\ &= ae^{j2\pi f(t-2R/c)}\left[e^{-j2\pi f D\sin\theta/c} + e^{+j2\pi f D\sin\theta/c}\right] \\ &= 2ae^{j2\pi f(t-2R/c)}\cos\left(\pi f D\sin\theta/c\right) \end{aligned} \tag{7.2}$$

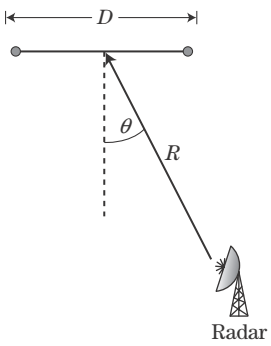

FIGURE 7-4 ■ Geometry for determining relative RCS of a dumbbell target.

RCS is proportional to the power of the composite echo, as shown in Section 6.5.1. Taking the squared magnitude of (7.2) leads to the result

$$\sigma \propto 4a^2 \left|\cos\left(2\pi f D \sin\theta/c\right)\right|^2 = 4a^2 \left|\cos\left(2\pi D \sin\theta/\lambda\right)\right|^2. \tag{7.3}$$

Equation (7.3) shows that the RCS is a function of both radar frequency and aspect angle. The larger the scatterer separation in terms of wavelengths, the more rapidly the RCS varies with angle or frequency. An exact calculation of the variation in RCS of the dumbbell target is plotted in Figure 7-5 for the case $D = 5\lambda$ and $R = 10{,}000D$. The plot has been normalized so that the maximum value corresponds to 0 dB. Notice the multi-lobed structure as the varying path lengths traversed by the echoes from the two scatterers cause them to shift between constructive and destructive interference. Also note that the maxima at aspect angles of 90° and 270° (the two "end-fire" cases) are the broadest, whereas the maxima at the two "broadside" cases of 0° and 180° are the narrowest. Figure 7-6 plots the same data in a more traditional polar format.

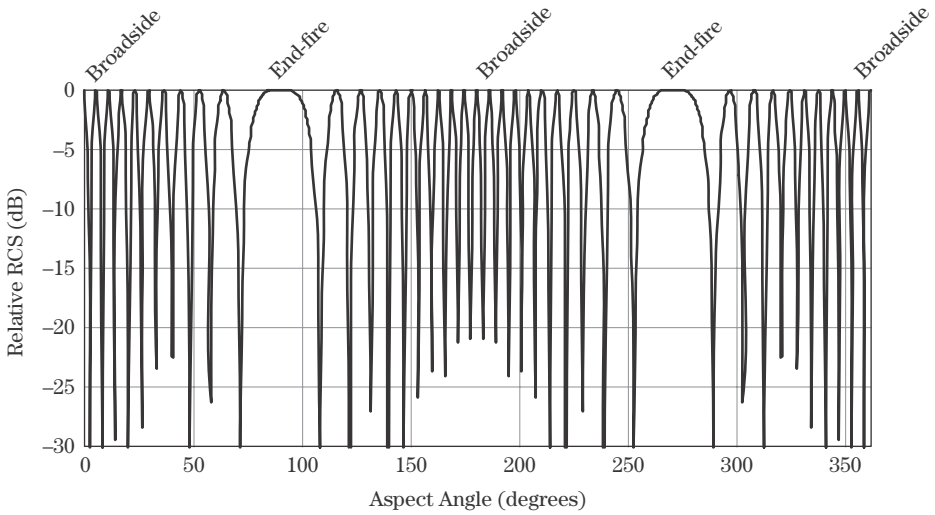

FIGURE 7-5 ■ Relative radar cross section of the dumbbell target of Figure 7-4 when $D = 5\lambda$ and $R = 10{,}000\,D$.

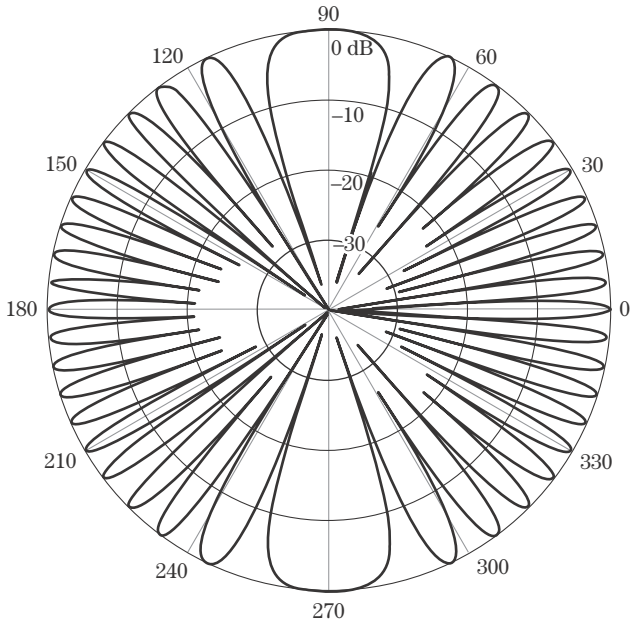

FIGURE 7-6 ■ Polar plot of the data of Figure 7-5.

7.3 | RADAR CROSS SECTION OF COMPLEX TARGETS

RCS variations become very complicated for complex targets having many scatterers of varying individual RCS. The relative RCS of a target with multiple scatterers can be computed using a generalization of (7.2). Suppose there are N scatterers, each with its own RCS σ_i, located at ranges R_i from the radar. The complex voltage of the echo will be, to within a proportionality constant,

$$\begin{aligned} y(t) &= \sum_{i=1}^{N} \sqrt{\sigma_i}\, e^{j2\pi f\left(t-2R_i/c\right)} \\ &= e^{j2\pi f t} \sum_{i=1}^{N} \sqrt{\sigma_i}\, e^{-j4\pi f R_i/c} \\ &= e^{j2\pi f t} \sum_{i=1}^{N} \sqrt{\sigma_i}\, e^{-j4\pi R_i/\lambda} \end{aligned} \tag{7.4}$$

The RCS σ is proportional to $|y|^2$. Define the echo *amplitude* as

$$\varsigma \equiv |y| = \left| \sum_{i=1}^{N} \sqrt{\sigma_i}\, e^{-j4\pi R_i/\lambda} \right| \tag{7.5}$$

and the target RCS as

$$\sigma = \varsigma^2 = \left| \sum_{i=1}^{N} \sqrt{\sigma_i}\, e^{-j4\pi R_i/\lambda} \right|^2 \tag{7.6}$$

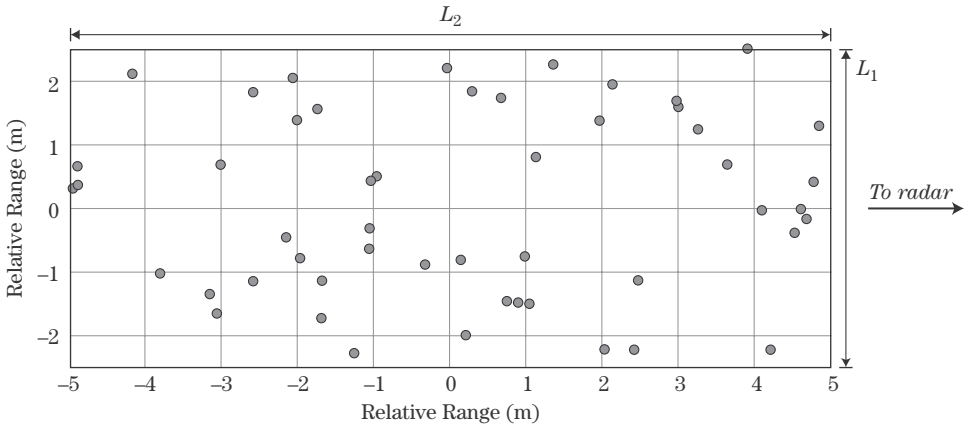

FIGURE 7-7 ■ Random distribution of 50 scatterers used to obtain Figure 7-8. See text for additional details.

While the previous equations implicitly assume a continuous wave (CW) radar, they also apply to a pulsed system so long as all the scatterers are contained in a single resolution cell so that all contribute to the receiver output simultaneously at a time corresponding to the nominal range to the target.

Figure 7-7 shows a "target" consisting of 50 point scatterers randomly distributed within a rectangle 5 meters wide and 10 meters long. The RCS of each individual point scatterer is a constant, $\sigma_i = 1.0$. Figure 7-8 shows the relative RCS, computed at 1 degree increments using (7.6), which results when this target is viewed 10 km from its center at a frequency of 10 GHz. Zero degrees corresponds to the radar being located to the right of the target, as indicated by the arrow. The dynamic range of the received power and thus the RCS is similar to that of the simple dumbbell target, but the lobing structure is much more complicated. A target whose RCS varies strongly with aspect angle or frequency is called a *fluctuating target*.

This complicated behavior observed for even moderately complex targets means that calculations of detection performance would be very sensitive to radar-target aspect angle because of the large variations of RCS and therefore of signal-to-noise ratio (SNR). Such calculations would be both complicated and of limited utility, since it would be difficult to know either the target RCS pattern or the radar-target aspect angle accurately enough to use such detailed data. It is much more practical and ultimately more useful to develop

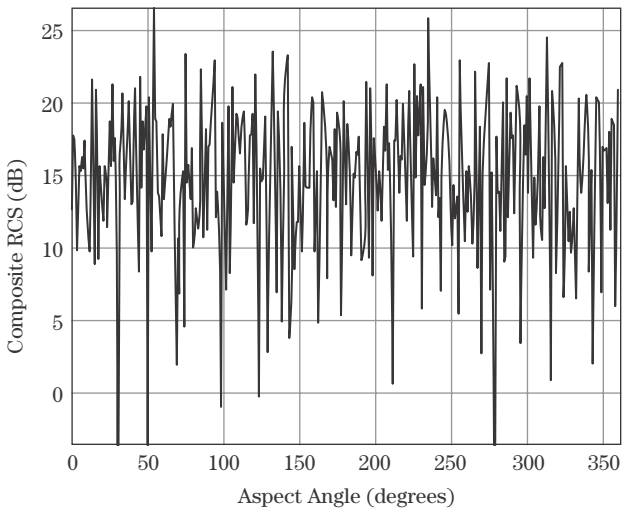

FIGURE 7-8 ■ Relative RCS of the complex target of Figure 7-7 at a range of 10 km and radar frequency of 10 GHz.

"average" performance based on a simpler model of the target RCS. This argument leads to the use of a statistical description for radar cross section [1–3] in which the composite RCS σ of the scatterers within a single resolution cell is considered to be a random variable with a specified *probability density function* (PDF). The radar range equation, or RCS modeling as described in Chapter 6, is used to estimate the mean RCS from received echo power measurements, and one of a variety of standard PDFs is used to describe the statistical variations of the RCS.

It is important to realize that using a statistical model for RCS does not imply that the actual RCS of the target is random. If it was possible to describe the target surface shape and materials in enough detail, and in addition to identify the radar-target aspect angle accurately enough, then the RCS could in principle be computed accurately using the techniques of the previous chapter. Statistical models are used because RCS behavior, even for relatively simple targets like the previous examples, is extremely complex and very sensitive to aspect angle. Combined with the uncertainty of aspect angle, particularly before a target is detected, it is much more practical to use a statistical model as a simple way to capture the complexity of the target RCS.

7.4 | STATISTICAL CHARACTERISTICS OF THE RCS OF COMPLEX TARGETS

7.4.1 RCS Distributions

Consider a target consisting of a large number of individual scatterers (similar to that of Figure 7-7) randomly distributed in space and each with approximately the same individual RCS. The phase of the echoes from the various scatterers can then be assumed to be a random variable distributed uniformly on $(0,2\pi)$. Under these circumstances, the central limit theorem guarantees that the real and imaginary parts of the composite echo can each be assumed to be independent, zero mean Gaussian random variables with the same variance, say α^2 [1,2]. In this case, the squared-magnitude σ has an exponential PDF [4]:

$$p(\sigma) = \begin{cases} \dfrac{1}{\bar{\sigma}} \exp\left[\dfrac{-\sigma}{\bar{\sigma}}\right], & \sigma \geq 0 \\ 0, & \sigma < 0 \end{cases} \tag{7.7}$$

where $\bar{\sigma} = 2\alpha^2$ is the mean value of the RCS σ.[1] The amplitude voltage, $\varsigma = \sqrt{\sigma}$ (more appropriate to a radar using a linear, rather than square law, detector), has a Rayleigh PDF:

$$p(\varsigma) = \begin{cases} \dfrac{2\varsigma}{\bar{\sigma}} \exp\left[\dfrac{-\varsigma^2}{\bar{\sigma}}\right], & \varsigma \geq 0 \\ 0, & \varsigma < 0 \end{cases} \tag{7.8}$$

While the Rayleigh/exponential model is strictly accurate only in the limit of a very large number of scatterers, in practice it can be a good model for a target having as few as 10 or 20 significant scatterers. Figure 7-9 compares a histogram of the RCS values from Figure 7-8 (after conversion from the decibel scale back to a linear scale) to an exponential curve of the form (7.7) having the same mean $\bar{\sigma}$. Even though only 50 scatterers are used,

[1]Note that this PDF applies to the RCS in linear scale units of m^2, not to decibel scale units of dBsm.

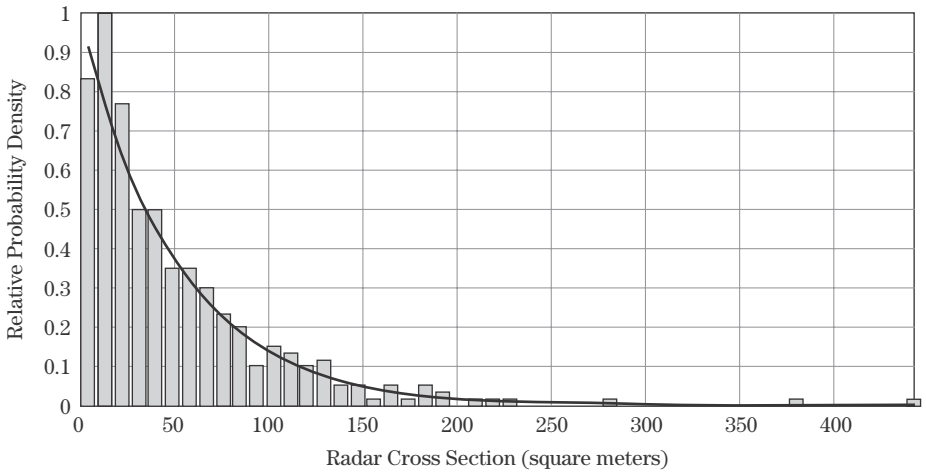

FIGURE 7-9 ■ Histogram of linear-scale RCS data of Figure 7-8.

the fit of the total RCS histogram to the exponential distribution is quite good. This same effect is observed when the randomly distributed scatterers also have random individual cross sections drawn from the same Gaussian distribution, a somewhat more general and plausible situation than the approximately fixed-RCS case.

Many radar targets are not well modeled as an ensemble of equal-strength scatterers, so a variety of other PDFs have been advocated and used for modeling target RCS. Table 7-1 summarizes several of the more common models. The mean value $\bar{\sigma}$ of RCS is given for each case in which the PDF is not written explicitly in terms of $\bar{\sigma}$. The variance var(σ) is also given for each case. The naming terminology can be confusing, because in some cases the name traditionally applied to the distribution of RCS σ is actually that of the density function of the corresponding amplitude, ζ. For example, the exponential RCS distribution of (7.7) is sometimes referred to as the Rayleigh model, because the amplitude (square root of the RCS) follows the Rayleigh PDF of equation (7.8).

Figure 7-10 is the histogram of an RCS versus aspect angle data set for a 20-scatterer target, but with an additional dominant scatterer added at a random location. The noncentral chi-square distribution with two degrees of freedom is the exact PDF for this case but is considered somewhat difficult to work with because the expression for the PDF contains a Bessel function. The fourth-degree chi-square is a more analytically tractable approximation that is commonly used. This PDF is given by

$$p(\sigma) = \begin{cases} \dfrac{4\sigma}{\bar{\sigma}^2} \exp\left[\dfrac{-2\sigma}{\bar{\sigma}}\right], & \sigma \geq 0 \\ 0, & \sigma < 0 \end{cases} \tag{7.9}$$

The first two central moments (mean and variance) of the two PDFs are equal when the RCS of the dominant scatterer is $1 + \sqrt{2} \approx 2.414$ times that of the sum of the radar cross sections of the small scatterers. The data in Figure 7-10 were computed using this ratio. The fourth-degree chi-square PDF with the same mean RCS overlaid on the histogram shows that the observed RCS data are a good fit to the theoretical model provided the ratio of dominant to small scatterers is correct.

The exponential and fourth-degree chi-square PDFs are the two most traditional models for target RCS. They are the PDFs used as part of the common *Swerling models* of RCS that will be introduced in Section 7.5.1. Both are special cases of a chi-square density of

TABLE 7-1 ■ Common Statistical Models for Radar Cross Section

Model Name	PDF for RCS σ	Comment
Nonfluctuating, Marcum, Swerling 0, or Swerling 5	$p(\sigma) = \delta_D(\sigma - \bar{\sigma})$ $\text{var}(\sigma) = 0$	Constant echo power, e.g. calibration sphere or perfectly stationary reflector with no radar or target motion.
Exponential (chi-square of degree 2)	$p(\sigma) = \frac{1}{\bar{\sigma}} \exp\left[\frac{-\sigma}{\bar{\sigma}}\right]$ $\text{var}(\sigma) = \bar{\sigma}^2$	Many scatterers, randomly distributed, none dominant. Used in Swerling case 1 and 2 models.
Chi-square of degree 4	$p(\sigma) = \frac{4\sigma}{\bar{\sigma}^2} \exp\left[\frac{-2\sigma}{\bar{\sigma}}\right]$ $\text{var}(\sigma) = \bar{\sigma}^2/2$	Approximation to case of many small scatterers + one dominant, with RCS of dominant equal to $1+\sqrt{2}$ times the sum of RCS of others. Used in Swerling case 3 and 4 models.
Chi-square of degree $2m$, Weinstock	$p(\sigma) = \frac{m}{\Gamma(m)\,\bar{\sigma}} \left[\frac{m\sigma}{\bar{\sigma}}\right]^{m-1} \exp\left[\frac{-m\sigma}{\bar{\sigma}}\right]$ $\text{var}(\sigma) = \bar{\sigma}^2/m$	Generalization of the two preceding cases. Weinstock cases correspond to $0.6 \le 2m \le 4$. Higher degrees correspond to presence of a more dominant single scatterer.
Weibull	$p(\sigma) = CB\sigma^{C-1} \exp\left[-B\sigma^C\right]$ $\bar{\sigma} = \Gamma\left(1 + 1/C\right) B^{-1/C}$ $\text{var}(\sigma) = B^{-2/C}\left[\Gamma\left(1+2/C\right) - \Gamma^2\left(1+1/C\right)\right]$	Empirical fit to many measured target and clutter distributions. Can have longer "tail" than previous cases.
Log-normal	$p(\sigma) = \frac{1}{\sqrt{2\pi}\, s\sigma} \exp\left[-\ln^2\left(\sigma/\sigma_m\right)/2s^2\right]$ $\bar{\sigma} = \sigma_m \exp\left(s^2/2\right)$ $\text{var}(\sigma) = \sigma_m^2 \exp\left(s^2\right)\left[\exp\left(s^2\right) - 1\right]$	Empirical fit to many measured target and clutter distributions. "Tail" is longest of previous cases. σ_m is the median value of σ.

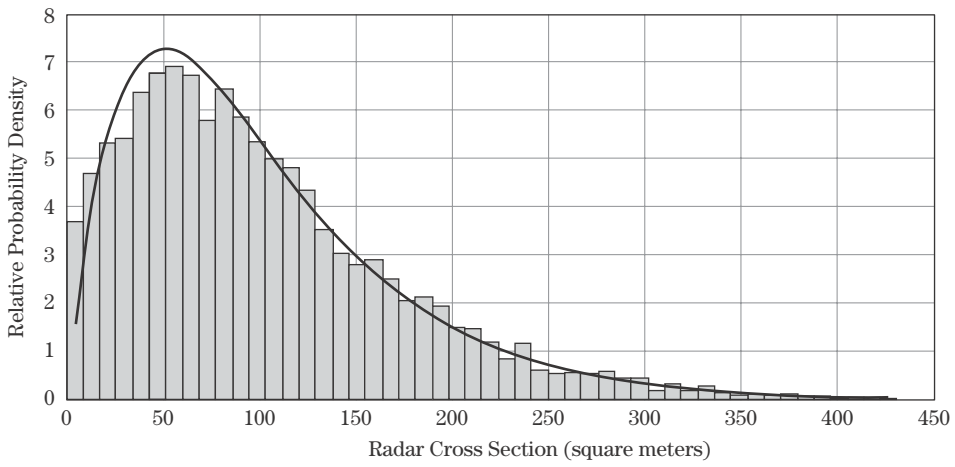

FIGURE 7-10 ■ Comparison of a fourth-degree chi-square PDF and the histogram of linear-scale RCS data for one dominant scatterer with many small scatterers. See text for details.

degree $2m$, where m is sometimes called the "duo-degree" of the density. This PDF is

$$p(\sigma) = \begin{cases} \dfrac{m}{\Gamma(m)\bar{\sigma}} \left[\dfrac{m\sigma}{\bar{\sigma}}\right]^{m-1} \exp\left[\dfrac{-m\sigma}{\bar{\sigma}}\right], & \sigma \geq 0 \\ 0, & \sigma < 0 \end{cases} \tag{7.10}$$

The exponential corresponds to $m = 1$, while the fourth-degree chi-square corresponds to $m = 2$.

The definition of the fourth-degree chi-square PDF as shown in equation (7.9) and Table 7-1 is common in radar but is otherwise somewhat nonstandard terminology. A chi-square of degree N is usually considered in the more general statistical literature to be a special case of the *gamma PDF*, which has two parameters α and β:

$$p(\sigma; \alpha, \beta) = \begin{cases} \dfrac{\sigma^{\alpha-1}}{\beta^{\alpha}\Gamma(\alpha)} e^{-\sigma/\beta}, & \sigma \geq 0 \\ 0, & \sigma < 0 \end{cases}, \tag{7.11}$$

Specifically, the conventional fourth-degree chi-square is obtained when $N = 4$, so $\alpha = 2$ and $\beta = 2$. However, the PDF in equation (7.9) is obtained from (7.11) with $\alpha = 2$ and $\beta = \bar{\sigma}/2$, which implies $N = 4$ but does not have $\beta = 2$. The more general form of the so-called shape parameter, β, is necessary to allow the mean of the distribution to be set to any desired value.

The chi-square of degree $2m$ in equation (7.10) is obtained by letting $\alpha = m$ and $\beta = \bar{\sigma}/m$ in the gamma PDF. Use of the gamma PDF to generalize the original chi-square models and to represent a wider range of target behavior was first proposed by Swerling in 1966 (reprinted in [6]). Another example of this generalization is the Weinstock models [7], which are chi-square PDFs with degrees between 0.6 and 4 that provide the ability to fit a range of dominant-to-small scatterer ratios from about 0.03 to $1 + \sqrt{2}$. For targets having stronger dominant scatterers, the non-central chi-square PDF is a better fit.

The Rayleigh/exponential function is an example of a *one-parameter PDF*; specifying only one parameter, the mean $\bar{\sigma}$, completely specifies the PDF. In particular, the variance of the PDF is related directly to its mean, as shown in Table 7-1. The chi-square models of a given degree are also one-parameter PDFs. In contrast, the Weibull and log-normal are examples of *two-parameter PDFs*. The shape of the PDF is determined by two independent parameters (B and C for the Weibull; σ_m and s for the log-normal). Consequently, their mean and variance can be adjusted independently so that two-parameter distributions can adequately fit a wider range of measured data distributions. For example, Figure 7-11 shows three variants of the log-normal distribution. All have the same mean of 1.0, but the variances are 0.2, 0.5, and 1.0. As the variance increases, the "tail" of the PDF lengthens; this is more readily evident in Figure 7-11b, which plots the PDFs on a log scale. Longer PDF tails represent a greater probability of higher RCS echoes.

Estimating the mean of a one-parameter distribution also provides the information needed for an estimate of the variance. For the two-parameter case, separate estimates of the mean and variance must be computed. This distinction is important in the design of automatic detection algorithms in Chapter 16.

The choice of PDF for modeling RCS fluctuations directly affects the estimation of detection performance, as will be seen in Chapter 15. Figure 7-12a compares the Rayleigh, fourth-degree chi-square, Weibull, and log-normal density functions when all have the same RCS variance of 0.5 and all except the exponential have a mean of 1.0.

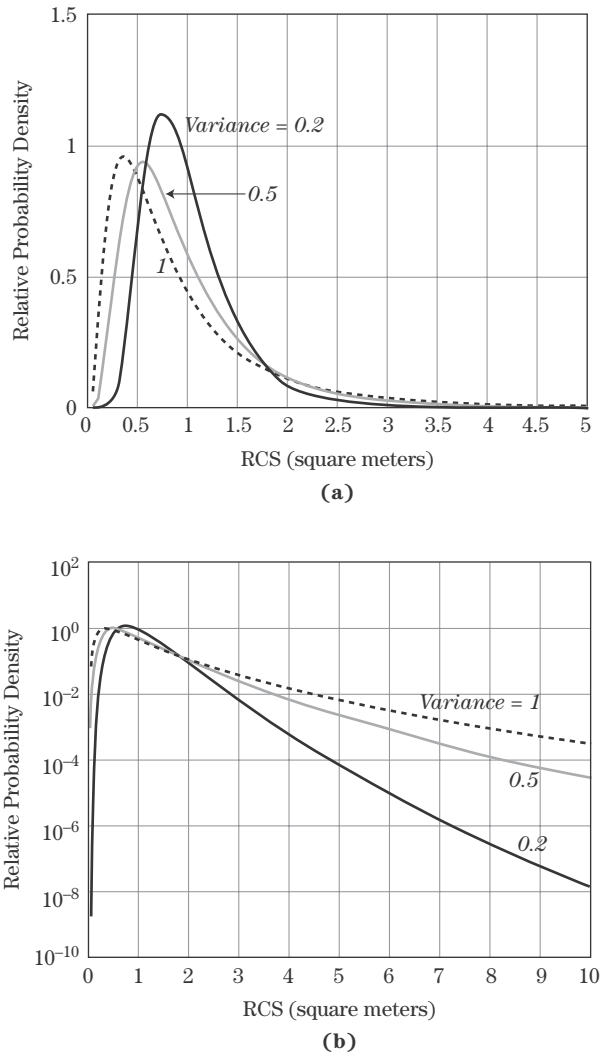

FIGURE 7-11 ■ Log-normal PDFs with mean = 1 and variances = 0.2, 0.5, and 1. (a) Linear scale. (b) Log scale, showing detail of the PDF "tails."

(Because it is a one-parameter distribution with its mean and variance always equal, the exponential distribution in the figure has a mean of 0.5). Figure 7-12b repeats the same data on a semilogarithmic scale so that the behavior of the PDF "tails" is more evident. The exponential PDF is somewhat unique, since it doesn't have a distinct peak near the RCS mean as the other three densities do. Each of the others does have a distinct peak, making each suitable for distributions with one or a few dominant scatterers. For the parameters shown, the Weibull has a broader peak and more rapidly decaying tail than does the chi-square of degree 4, while the log-normal has both the narrowest peak and the longest tail of any of the distributions shown. However, the sharpness of the peak and the length of the PDF tail can be varied for both the Weibull and log-normal by adjusting their variance.

Not all targets exhibit RCS fluctuations. Targets whose RCS is modeled as a constant, independent of aspect angle are called *nonfluctuating* targets; they are also sometimes called *Marcum* targets. Examples include the conducting sphere and, so long as the aspect angle doesn't vary too much from its axis of symmetry, the various corner reflectors.

Most radar analysis and measurement programs emphasize RCS measurements, since received power is proportional to RCS. Sometimes the corresponding amplitude voltage,

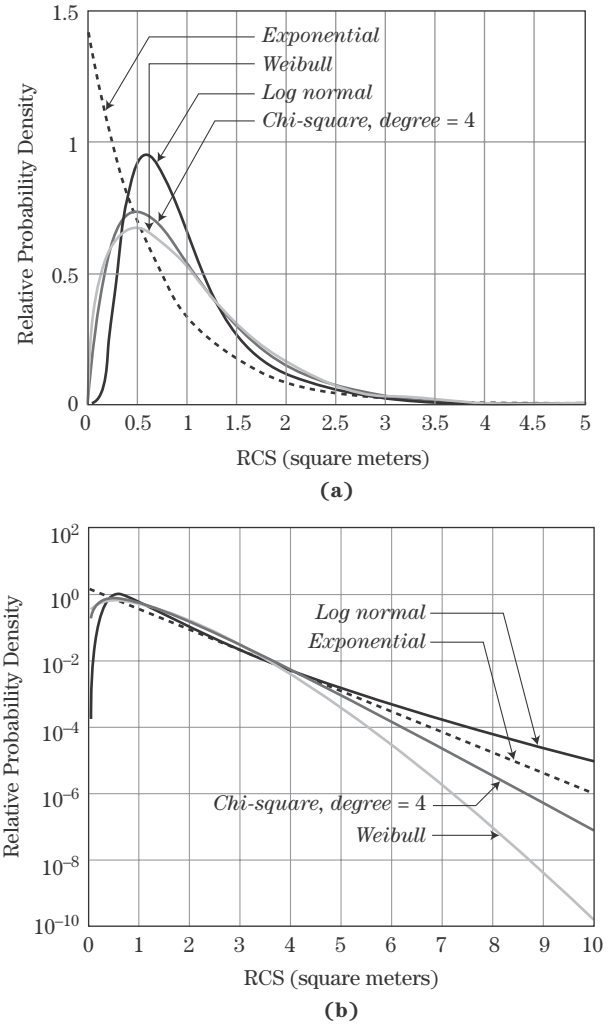

FIGURE 7-12 ■ Comparison of five models for the probability density function of radar cross section with the same mean (except for the exponential) and variance. See text for additional details. (a) Linear scale. (b) Log scale, showing detail of the PDF "tails."

ς, is of interest, particularly for use in simulations where equation (7.4) is used explicitly to model the composite echo from a multiple scatterer target. The probability density function for the amplitude is required to properly model the probabilistic variations of the complex sum. The PDF of ς is easily derived from the PDF of σ using basic results of random variables [4]. Specifically, the PDF of ς is related to that of the RCS σ by

$$p_{\varsigma}(\varsigma) = 2\varsigma p_{\sigma}(\varsigma^2) \tag{7.12}$$

Equation (7.12) can be used to write the voltage PDFs by inspection from Table 7-1. The results, given in Table 7-2, are expressed in terms of the parameters of the corresponding RCS distribution from Table 7-1. Note that the nonfluctuating, Weibull, and log-normal RCS distributions all result in distributions of the same type (but with one or more parameters changed) for the voltage. Again, note that the voltage in the Rayleigh/exponential case is Rayleigh distributed, explaining the name.

7.4.2 RCS Correlation Properties

As has been seen, the RCS of a complex target varies with both transmitted frequency and aspect angle. Another important characteristic of a target's signature is the *correlation*

TABLE 7-2 ■ Voltage Distributions Corresponding to Common Statistical Models of Radar Cross Section

RCS Model Name	PDF for Voltage ζ	Description of Voltage Model
Nonfluctuating, Marcum, Swerling 0, or Swerling 5	$p(\varsigma) = \delta_D\left(\varsigma - \sqrt{\bar{\sigma}}\right)$ $\bar{\varsigma} = \sqrt{\bar{\sigma}}, \quad \text{var}(\sigma) = 0$	Also nonfluctuating model
Exponential (chi-square of degree 2)	$p(\varsigma) = \frac{2\varsigma}{\bar{\sigma}} \exp\left[\frac{-\varsigma^2}{\bar{\sigma}}\right]$ $\bar{\varsigma} = \frac{1}{2}\sqrt{\pi\bar{\sigma}}, \quad \text{var}(\varsigma) = \bar{\sigma}\left(1 - \pi/4\right)$	Rayleigh distribution
Chi-square of degree 4	$p(\varsigma) = \frac{8\varsigma^3}{\bar{\sigma}^2} \exp\left[\frac{-2\varsigma^2}{\bar{\sigma}}\right]$ $\bar{\varsigma} = \frac{3}{4}\sqrt{\pi\bar{\sigma}}, \quad \text{var}(\varsigma) = \left(1 - \frac{9}{32}\pi\right)\bar{\sigma}$	Chi-distribution of degree 4
Chi-square of degree $2m$, Weinstock	$p(\varsigma) = \frac{2\varsigma m}{\Gamma(m)\bar{\sigma}}\left(\frac{m\varsigma^2}{\bar{\sigma}}\right)^{m-1} \exp\left[-\frac{m\varsigma^2}{\bar{\sigma}}\right]$ $\bar{\varsigma} = \sqrt{\frac{\bar{\sigma}}{m}}, \quad \text{var}(\varsigma) = \bar{\sigma}\left[1 - \frac{1}{m}\left(\Gamma(m+0.5)/\Gamma(m)\right)^2\right]$	Chi-distribution of degree $2m$
Weibull	$p(\varsigma) = 2CB\varsigma^{2C-1} \exp\left[-B\varsigma^{2C}\right]$ $\bar{\varsigma} = \Gamma\left(1 + 1/2C\right) B^{-1/2C}$ $\text{var}(\varsigma) = \left[\Gamma\left(1 + 1/C\right) - \Gamma^2\left(1 + 1/2C\right)\right] B^{-1/2C}$	Also Weibull, one parameter changed ($C \to 2C$).
Log-normal	$p(\varsigma) = \frac{2}{\sqrt{2\pi}\, s\varsigma} \exp\left[-2\ln^2\left(\varsigma/\sqrt{\sigma_m}\right)^2 / s^2\right]$ $\bar{\varsigma} = \sqrt{\sigma_m} \exp\left(s^2/8\right)$ $\text{var}(\varsigma) = \sigma_m \exp\left(s^2/4\right)\left[\exp\left(s^2/4\right) - 1\right]$	Also log-normal, both parameters changed ($s \to s/2, \sigma_m \to \sqrt{\sigma_m}$).

"length" in time, frequency, and angle. This is the change in time, frequency, or angle required to cause the echo amplitude to decorrelate to a specified degree. If a rigid target such as a building is illuminated with a series of identical radar pulses and there is no motion between the radar and target, each pulse will result in the same received complex voltage ς (ignoring receiver noise). If there is motion between the two, however, the relative path length between the radar and the various scatterers comprising the target will change, causing the composite echo amplitude to fluctuate, similar to the fluctuations shown in Figure 7-8. Changing the radar wavelength will also cause the relative phase of the contributing scatterers to change, producing the same effect, as will target vibration in some instances. Thus, for rigid targets, decorrelation of the RCS is induced by changes in range, aspect angle, and radar frequency.

Although the behavior of real targets can be quite complex, a sense of the change in frequency and angle required to decorrelate a target or clutter patch can be obtained by the following simple argument. Consider an idealized target consisting of a uniform line array of point scatterers tilted at an angle θ with respect to the line of sight to the radar and separated by Δx from one another, as shown in Figure 7-13. For simplicity, assume an odd number $2M + 1$ of scatterers indexed from $-M$ to $+M$ as shown. If the nominal

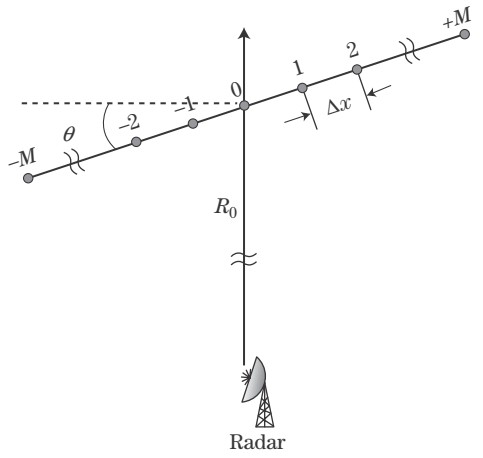

FIGURE 7-13 ■ Geometry for calculation of RCS correlation length in frequency and aspect angle.

distance to the radar, R_0, is much larger than the target extent (i.e., $R_0 \gg (2M+1)\Delta x$), then the range to the n-th scatterer is approximately

$$R_n \approx R_0 + n\,\Delta x \sin\theta \tag{7.13}$$

If the target is illuminated with the waveform $ae^{j\omega t}$, the received signal is

$$\begin{aligned} \bar{y}(t) &= \sum_{n=-M}^{M} ae^{j\omega(t-2R_n/c)} \\ &= ae^{j\omega(t-2R_0/c)} \sum_{n=-M}^{M} e^{-j4\pi n\,\Delta x\,\sin\theta\, f/c} \end{aligned} \tag{7.14}$$

To simplify the notation, define

$$\begin{aligned} z &= f\sin\theta \\ \alpha &= 4\pi\,\Delta x/c \end{aligned} \tag{7.15}$$

The new variable z includes both aspect angle and radar frequency. The signal $\bar{y}(t)$ can now be considered as a function $\bar{y}(t;z)$ of both t and z, and its autocorrelation can be computed with respect to the variable z. It can be shown that the deterministic autocorrelation function is [5]

$$s(\Delta z) = \frac{2\pi a^2}{\alpha} \frac{\sin\left[\alpha\,(2M+1)\,\Delta z/2\right]}{\sin\left[\alpha\,\Delta z/2\right]} \tag{7.16}$$

where Δz is the correlation lag in the z dimension.

One criterion for "decorrelation" is to choose the value of Δz corresponding to the first zero of the correlation function. This occurs when the argument of the numerator equals π. Using (7.15) and defining the target length $L = (2M+1)\Delta x$,

$$\Delta z = \frac{c}{2L} \tag{7.17}$$

Recall that $z = f\sin\theta$. To determine the decorrelation angle, fix the transmitted frequency f so that $\Delta z = f(\Delta\sin\theta)$. Assuming θ is small (i.e., the radar is near broadside),

$\Delta \sin\theta \approx \Delta\theta$. Equation (7.17) then becomes the desired result for the angle required to decorrelate the echo amplitude:

$$\Delta\theta = \frac{c}{2Lf} = \frac{\lambda}{2L} \tag{7.18}$$

For rigid targets, equation (7.18) estimates the amount of aspect angle rotation required to decorrelate the target echoes. Aspect angle changes will occur because of motion between the radar and the target. For instance, an airliner flying past a commercial airport presents a constantly changing aspect to the airport surveillance radar as it flies through the airspace. The amount of time over which the aircraft echoes decorrelate is simply the amount of time it takes to change the aspect angle by $\Delta\theta$ radians, which depends on the details of the relative geometry and velocity of the radar and target.

The frequency step required to decorrelate the target is obtained by fixing the aspect angle θ so that $\Delta z = \Delta f \sin\theta$. The result is

$$\Delta f = \frac{c}{2L\sin\theta} \tag{7.19}$$

This is minimum when $\theta = 90^\circ$. Note that $L\sin\theta$ is the length of the target line array projected along the radar boresight. The value of Δf required to decorrelate the target is usually modest. For example, if the projected target size $L\sin\theta = 10$ m, $\Delta f = 15$ MHz.

This result can be generalized slightly to apply it to an $L_1 \times L_2$ meter target such as the 5 m × 10 m target used previously. The size of this rectangular target as projected along the line of sight (LOS) when the radar is at an aspect angle of θ radians measured from horizontal is the sum of the projection of each side of the target along the LOS, which is $L_1 \sin\theta + L_2 \cos\theta$. Using this in equation (7.19) gives the frequency decorrelation step size as

$$\Delta f = \frac{c}{2\left(L_1|\sin\theta| + L_2|\cos\theta|\right)} \tag{7.20}$$

This result assumes that the target lies entirely within a single range bin. If the range resolution, ΔR, is less than the target extent along the LOS, the required step size is $c/(2\Delta R)$.

As an example, consider a target the size of an automobile, about 5 m long. At L-band (1 GHz), the target signature can be expected to decorrelate in $(3 \times 10^8)/(2 \times 5 \times 10^9) =$ 30 mrad of aspect angle rotation, about 1.7°, while at W-band (95 GHz), this is reduced to only 0.018°. Equation (7.19) predicts the frequency step required for decorrelation with an aspect angle of 45° is 42.4 MHz. This result does not depend on the transmitted frequency.

As another example, the autocorrelation in angle of the simulated data of Figure 7-8 is shown in Figure 7-14, using only the data for aspect angles over a range ±3°. Each of the two autocorrelation functions is the average of the data from 20 different random targets, each having 20 randomly placed scatterers in a 5 m × 10 m box, similar to the simulation previously described. The black curve is the autocorrelation of the data around a nominal boresight orthogonal to the 5 m side of the target, while the gray data are the autocorrelation of the data viewed from the 10 m side. These look angles correspond to viewing the target nominally from the right and from the top in Figure 7-7. Viewed from the right, $L = 5$ m orthogonal to the LOS and $f = 10$ GHz gives an expected decorrelation interval in angle of 0.17°; viewed from the top, $L = 10$ m and the expected decorrelation angle is 0.086°. These expected decorrelation intervals are marked by the vertical dashed lines in Figure 7-14. This figure shows that in both cases, the correlation function drops to zero at the expected amount of change in the aspect angle.

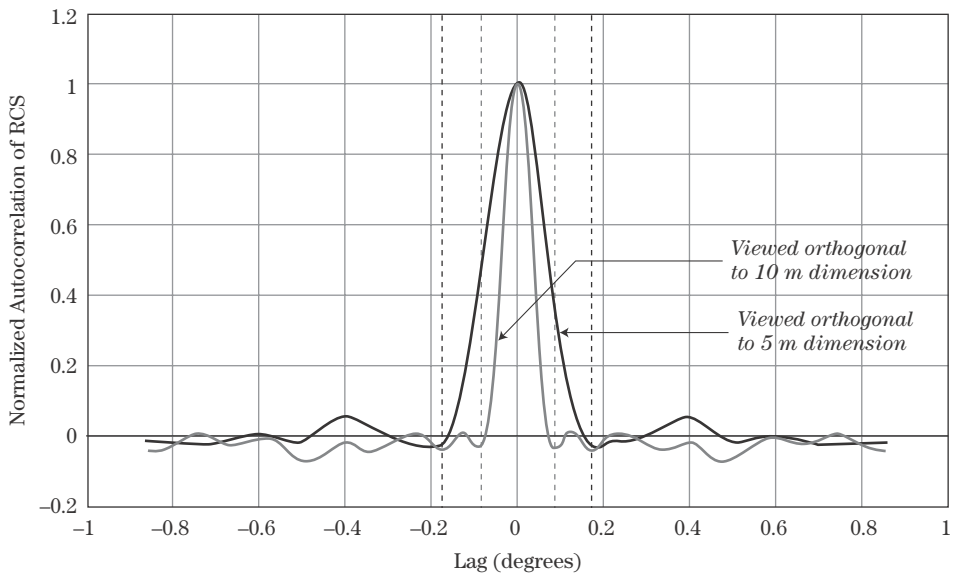

FIGURE 7-14 ■ Decorrelation in angle of RCS of target from Figure 7-8. See text for details.

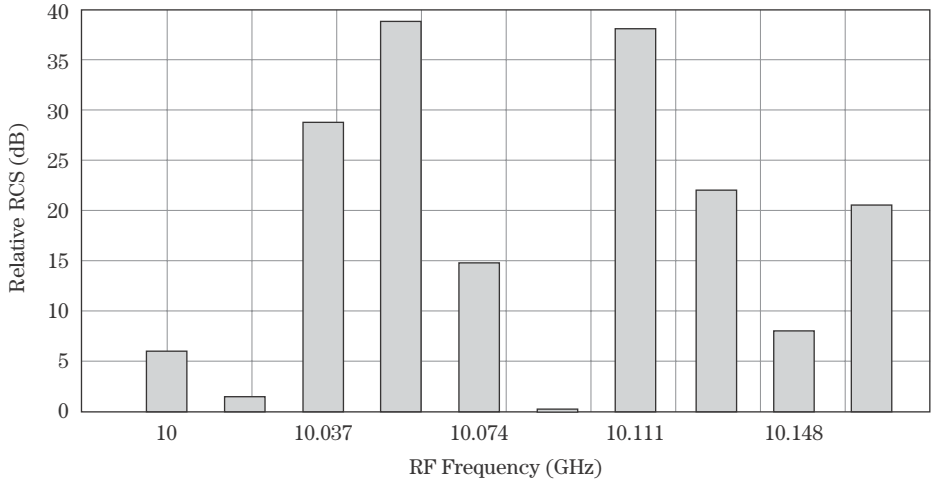

FIGURE 7-15 ■ Variation in RCS due to frequency agility for a constant viewing angle. See text for details.

Some systems deliberately change the radar frequency from pulse to pulse to decorrelate the target returns, a process called *frequency agility* [8]. As will be seen in Chapter 15, frequency agility can significantly improve the probability of detection for some systems and targets.

Figure 7-15 illustrates the ability of frequency agility to force RCS variations. A 20-scatterer, 5 m × 10 m random target similar to those previously described was observed from a fixed aspect angle of 20°. If the same radiofrequency (RF) was used for each pulse, the RCS would be exactly the same on each pulse. However, in this case the RF was increased by 18.48 MHz (calculated from equation (7.20)) from one pulse to the next, starting at 10.0 GHz. The resulting relative RCS measurements vary by 38 dB, a factor of about 6,300.

The results of equations (7.18) and (7.19) are based on a highly simplified target model and an assumption about what constitutes decorrelation. For example, defining decorrelation to be the point at which the correlation function first drops to 1/2 or 1/*e* of its

peak results in a smaller estimate of the required change in angle or frequency to decorrelate the target. Also, many radars operate on the magnitude squared of the echo amplitude rather than on the magnitude, as has been assumed in this derivation. A square law detector produces a correlation function proportional to the square of equation (7.16) [9]. The first zero therefore occurs at the same value of Δz, and the previous conclusions still apply. However, if a different definition of decorrelation is used (such as the 50% decorrelation point), the required change in Δz is less for the square law than for the linear detector.

7.5 TARGET FLUCTUATION MODELS

7.5.1 Swerling Models

An extensive body of radar detection theory results have been built up using the four *Swerling models* of target RCS fluctuation [2,3,10-12]. Swerling models are intended to address the common problem of making a detection decision based on a block of N envelope-detected echo samples from a given range-angle or range-Doppler resolution cell. To see one reason why detection based on a block of N samples (instead of just one) is of interest, imagine a ground-based surveillance radar used to detect aircraft. Suppose the radar antenna rotates at a constant angular velocity Ω radians/sec with a 3 dB azimuth beamwidth of θ_3 radians and a pulse repetition frequency (PRF) of PRF Hz. The geometry is shown in Figure 7-16. Although some echo energy from the target is received in the appropriate range bin on every pulse through the antenna sidelobes, significant returns are received only when the target is in the antenna mainlobe. Every complete 360° sweep of the antenna results in a new set of $N = (\theta_3/\Omega) \times PRF$ mainbeam samples, all potentially containing significant target echoes. It is desirable to use all of this target data for detection, not just a single pulse.

This is not the only way a block of N-related pulse echoes can arise. Many modern systems are designed to transmit coherent bursts of pulses at a constant pulse repetition frequency, often with the antenna staring in a fixed direction. The time interval

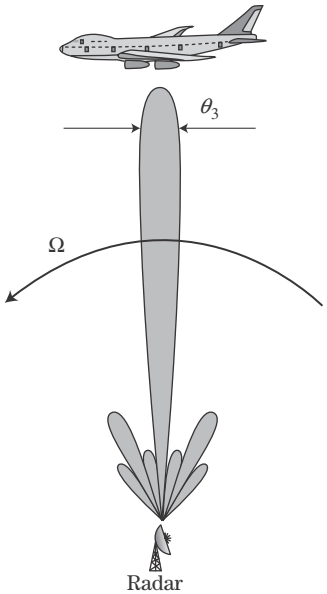

FIGURE 7-16 ■ Rotating antenna rationale for Swerling model decorrelation assumptions. Echoes from a given target are collected in blocks. Each rotation of the antenna results in a new block, and each block contains multiple pulse returns.

$N/PRF = N \times PRI$ required for this measurement is called a *coherent processing interval* (CPI).[2] The system may then repeat the entire measurement in the same or a different look direction, may change the PRF to make a related measurement, or may make any of a number of other changes in collecting the next CPI of data. This *N*-pulse burst is a common waveform well suited to Doppler measurements, adaptive interference suppression, and imaging applications. It will arise frequently in subsequent chapters. When multiple samples from the same range bin are combined coherently, the result is treated as a single sample for detection purposes. For example, if Doppler processing is performed as described in Chapter 17, the output would be one sample for each range-Doppler bin. However, the same data can also be combined noncoherently, in which case it again fits the model of detection based on *N* amplitude or power samples.

To analyze the detection performance obtainable with this block of *N* samples, it is necessary to model their joint statistics. The samples are assumed to be identically distributed but not necessarily independent. Thus, the amplitude of each individual pulse echo from the range bin of interest will be modeled by the same probability density function, typically one of those listed in Table 7-2. However, this still leaves the question of whether each of the *N* echo amplitudes is the same within a given antenna sweep, an independent random variable from the distribution, or something in between. This is a question of the *correlation* of the samples within the block of data.

The Swerling models are a combination of a specific probability density function for the echo powers and a specific assumption about the correlation of the *N* samples in a block. There are four Swerling models, formed from two choices for the PDF and two for the correlation behavior. The two density functions used by Swerling to describe RCS are the exponential and the chi-square of degree 4. As has been seen, the exponential model describes the behavior of a complex target consisting of many scatterers, none of which is dominant, while the fourth-degree chi-square adequately models targets having many scatterers of similar strength with one dominant scatterer, provided the ratio of the dominant to small scatterers is on the order of 2.4.

Swerling considered two bounding cases for the correlation properties of the block of *N* samples. The first assumes they are all perfectly correlated, so that all *N* echoes collected on one scan have the same value. This effectively assumes that the radar-target aspect angle varies by less than the $\Delta\theta$ of equation (7.18) over an interval of *N* PRIs. If the antenna scan time is greater than the target decorrelation time, the *N* new pulses collected on the next sweep will have the same value as one another also, but their value will be independent of the value measured on the first sweep. This case is referred to as *scan-to-scan decorrelation*. The second case assumes that each individual pulse on each sweep results in an independent random value for the amplitude, effectively assuming that the radar-target aspect angle varies by more than $\Delta\theta$ radians in one PRI, that frequency agility is used to ensure decorrelation, or both. This case is referred to as *pulse-to-pulse decorrelation*. The decorrelation properties of real data often fall between these extremes, but they are useful for bounding the detection results. It has been noted that relatively high pulse-to-pulse correlation coefficients, approximately 0.8 or more, are required before correlation has a major effect on detection performance, at least for exponential target RCS statistics [11].

[2]The term *CPI* is often used to refer to the block of data samples collected within the time interval as well as to the time interval itself.

TABLE 7-3 ■ Swerling Models

Probability Density Function of RCS	Decorrelation	
	Scan-to-Scan	Pulse-to-Pulse
Exponential	Case 1	Case 2
Chi-square, degree 4	Case 3	Case 4

The four combinations of the two choices for the PDF of the target power and the two choices for the decorrelation characteristics are denoted the "Swerling 1" through "Swerling 4" models of target fluctuation. Table 7-3 defines the four cases. In some references, the terminology is stretched to include the nonfluctuating target (Marcum) case as the "Swerling 0" or, less commonly, the "Swerling 5" model. Figure 7-17 illustrates a notional series of measurements from two different Swerling models. In each case, 10 pulses are received on each of three successive scans; the dead time between groups of

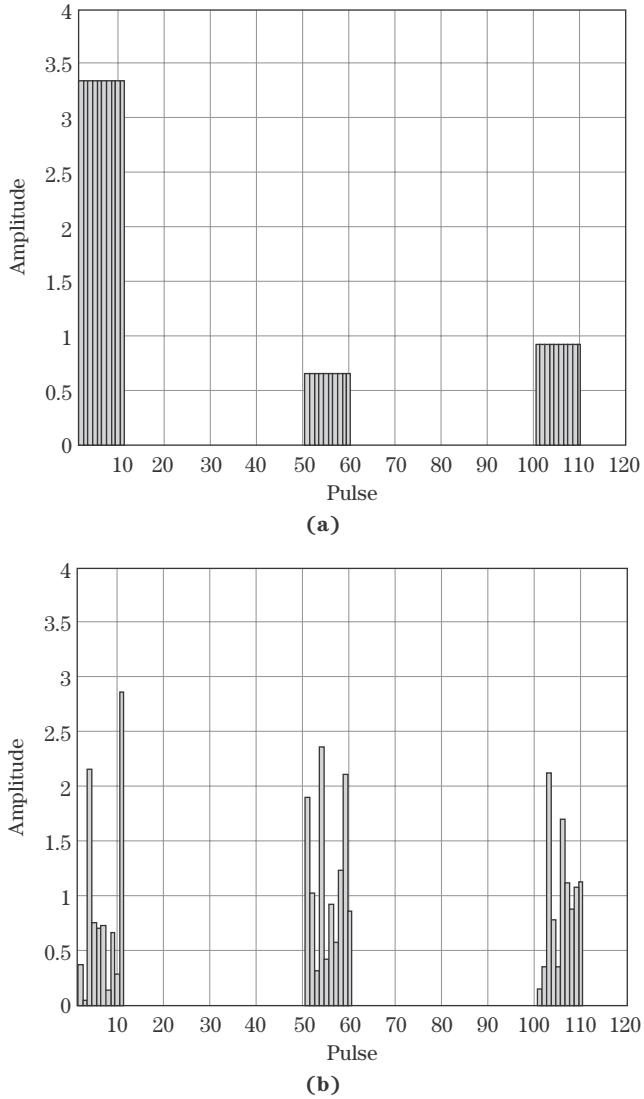

FIGURE 7-17 ■ Notional sequences of Swerling target samples. Results from three scans with 10 pulses per scan are shown. (a) Swerling case 1. (b) Swerling case 4.

pulses represents time in which the antenna is scanned in other directions so that the target is not in the antenna beam. Figure 7-17a represents Swerling case 1, which exhibits scan-to-scan decorrelation. Thus, within a scan, all 10 samples are the same, but that value changes from scan to scan according to an exponential distribution. Figure 7-17b is an example of the pulse-to-pulse decorrelation observed in Swerling case 4, where each individual sample is a new random value, in this case from a fourth-degree chi-square distribution. Chapter 15 develops exact and approximate formulas for the probability of detection and false alarm for the Swerling fluctuating target models and discusses the implications of the choice of target model.

Choosing a Swerling model for analysis requires that a choice be made between the two PDFs and between the two correlation models. To choose the PDF, the designer must have some knowledge about the RCS characteristics of the target of interest. Specifically, a judgment is needed as to whether the target RCS at the aspect angles of interest are likely to be dominated by one or two large scatterers or whether it is better described as the result of an ensemble of roughly equal scatterers. This decision is best based on measured data of the targets of interest at the appropriate frequencies, polarizations, and aspect angles, but such data are not always available. In many organizations and programs, there are well-established legacy practices for determining which Swerling or other target fluctuation model is appropriate for various classes of targets. However, care must be taken not to assume that models appropriate for use with one class of radar are necessarily valid for newer radars with different characteristics, for instance, higher RFs or much finer resolution.

The choice of the correlation model is primarily a matter of radar frequency, geometry, timeline, and the use of frequency agility. If the radar uses frequency agility to force decorrelation of the target echoes within the block of N samples, then a Swerling 2 or 4 model, depending on the selected PDF, should be chosen. If not, the designer must decide whether the aspect angle will change by more than $\Delta\theta$ radians, where $\Delta\theta$ is estimated using equation (7.18), during the collection of the block of N samples to be combined in the detection test. If not, scan-to-scan decorrelation (case 1 or 3) should be assumed. On the other hand, if the aspect angle changes by more than $\Delta\theta$ radians in one PRI, pulse-to-pulse decorrelation (case 2 or 4) should be selected. If the situation is likely to fall in between these extremes, calculations for both cases can be used to bound the range of detection results.

As an example, consider a 10 m long complex aircraft viewed with a stationary X-band (10 GHz) radar from a range of 30 km. The radar is not frequency agile. An exponential PDF is assumed due to the scattering complexity of the aircraft. The decorrelation angle estimated by equation (7.18) is 0.86° (1.5 mrad). Suppose the aircraft is flying at 200 m/s in a crossing direction (i.e., orthogonal to the radar LOS rather than directly toward or away from the radar). The angle between the radar and aircraft will change by 1.5 mrad when the aircraft has traveled $(0.0015)(30 \times 10^3) = 45$ m, which occurs in $45/200 = 225$ ms. Thus, if the radar collects a dwell of echoes from the target in less than 225 ms, the RCS would be expected to be fairly constant over the series of measurements and a Swerling 1 model should be assumed. If the PRI is longer than 225 ms, then a Swerling 2 model should be selected.

This example illustrates that very long PRIs would be required to decorrelate the data from pulse to pulse in many scenarios. For this reason, the Swerling 2 or 4 model is most often used with radars that employ frequency agility.

7.5.2 Extended Models of Target RCS Statistics

The strategy of the Swerling models can easily be extended to other target models. For example, one could define a model that uses a log-normal PDF for the target fluctuations with either pulse-to-pulse or scan-to-scan decorrelation to relate the N pulses in a block. Empirical observations have shown that such "long-tailed" distributions are often a better representation of observed radar data statistics than the traditional exponential and chi-square models, especially in high-resolution systems. Small resolution cells isolate one or a few scatterers, undermining the many-scatterer assumption of the traditional models and making large variations in observed RCS more likely as aspect or frequency changes. The approach to computing detection probabilities for such models is identical to that used with the Swerling models (see Chapter 15). However, the details are sometimes difficult to develop because the integrals of the PDFs are difficult to compute. Nonetheless, a number of results are available in the literature [e.g., 13].

Shnidman has proposed extending the Swerling models further by generalizing the gamma density underlying the traditional models to the noncentral gamma density [14]. This model allows for targets whose echo amplitudes exhibit a nonzero mean in the in-phase (I) or quadrature (Q) channels over a period of time on the order of N PRIs. Such a model is appropriate when the echoes contain one very steady component modulated by the echo from a number of smaller scatterers. This might happen, for instance, if echo from a large sea wave is modulated by rapidly varying surface ripples. A still further extension is to allow the nonzero mean component to itself fluctuate slowly, leading to what Shnidman calls the noncentral gamma-gamma density. The advantage of these extended models is that they introduce additional parameters that make it possible to more closely match the density function to experimentally observed statistics for a wide range of systems while maintaining the (relatively) tractable computational results obtainable with target models based on chi-square and gamma densities as opposed to log-normal or other density functions.

7.6 | DOPPLER SPECTRUM OF FLUCTUATING TARGETS

The correlation properties of a block of N target samples have implications for the Doppler spectrum of the target as well. Consider a possibly moving target, and ignore noise. The phase of the target echoes will change linearly from one sample to the next at a rate appropriate to the Doppler shift. If the target is either nonfluctuating or exhibits scan-to-scan decorrelation, the amplitude of the echoes will be constant or nearly so over the CPI. Thus, the slow-time target signal after demodulation to baseband will be of the form

$$y[m] = Ae^{j2\pi f_D mT}, \quad 0 \le m \le M-1 \tag{7.21}$$

where A is the nonfluctuating (constant) amplitude, f_D is the Doppler shift, T is the PRI, m is the pulse number, and M is the number of pulses in the CPI. The Doppler spectrum of this signal is a "digital sinc" function with a 3 dB width of $0.89/MT$ Hz (see Chapter 14 or [5]).

If the target echo power is fluctuating instead, the amplitude will no longer be a constant A but will vary pulse to pulse in some sequence $A[m]$ consistent with the PDF and

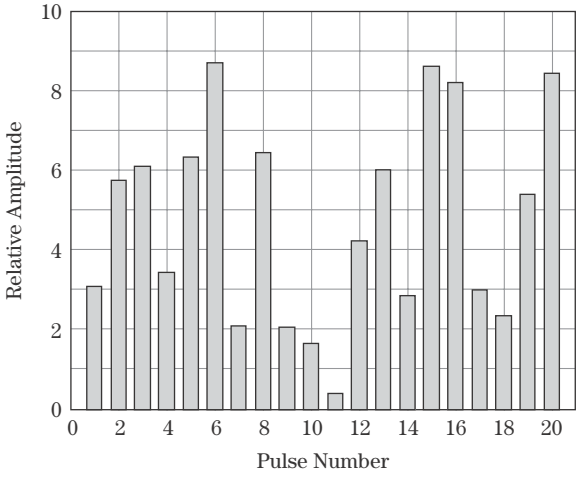

(a)

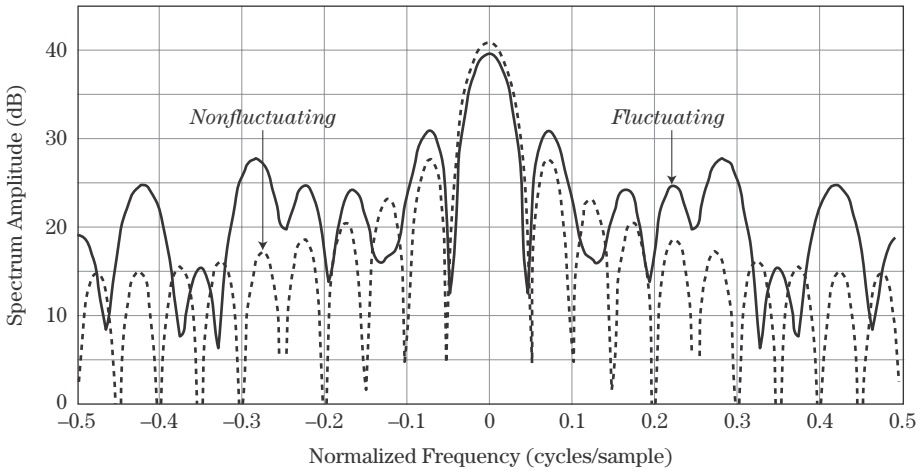

(b)

FIGURE 7-18 ■ Effect of amplitude fluctuations on target Doppler spectrum. (a) 20-pulse Rayleigh fluctuating amplitude sequence. (b) Spectrum of the fluctuating and nonfluctuating data.

correlation properties of the target amplitude. The Doppler spectrum of such a target will still be concentrated at the appropriate Doppler shift, but the nonzero bandwidth of the amplitude sequence $A[m]$ will spread the target spectrum. Figure 7-18 illustrates this effect. Figure 7-18a shows a sequence of amplitude (not power) measurements from a target with an exponential RCS distribution and pulse-to-pulse decorrelation (the Swerling 2 model). A stationary target (zero Doppler) is assumed without loss of generality. Figure 7-18b compares the spectrum of this fluctuating target with that of a nonfluctuating target with the same total energy in the data. Although the Doppler mainlobe is only slightly affected, significant energy is spread into the sidelobe regions of the response.

The Doppler spectrum of a complex target may also include discrete features due to moving parts on a target. For instance, a propeller-driven aircraft or a helicopter will have peaks in its Doppler spectrum corresponding not only to the radial velocity of the target as a whole but also to the velocity of the propeller or rotor tips as viewed from the radar. Similarly, a jet aircraft may introduce Doppler responses corresponding to the rotational speeds of the internal rotors of the jet engine. Ground vehicles may have additional Doppler

components from the rotational speed of the wheels of the vehicle. Several examples of such *microDoppler* signatures are given in [15]. In some cases, they can be useful for target classification or identification as discussed in Chapter 1.

7.7 FURTHER READING

Common current introductory textbooks on RCS generally give limited attention to modeling of complex target RCS variations. Some discussion of target fluctuations and statistical models can be found in Skolnik [16], Edde [17], Levanon [18], and Mahafza [19]. Skolnik's text also has a brief but useful discussion on how to choose between models. A good discussion of the scattering characteristics of complex targets with special emphasis on correlation properties is given in Chapter 5 of the text by Nathanson [15], though the data sources used are becoming dated. Good recent sources on generalized Swerling-type models and related detection calculations in modern terminology and notation are the series of papers by Shnidman [11–14].

7.8 REFERENCES

[1] Knott, E.F., Shaeffer, J.F., and Tuley, M.T., *Radar Cross Section*, 2d ed., SciTech Publishing, Raleigh, NC, 2004.

[2] Meyer, D.P., and Mayer, H.A., *Radar Target Detection*, Academic Press, New York, 1973.

[3] Swerling, P., "Probability of Detection for Fluctuating Targets," *IRE Transactions on Information Theory*, vol. IT-6, pp. 269–308, April 1960.

[4] Papoulis, A., and Pillai, S.U., *Probability, Random Variables, and Stochastic Processes*, 4th ed., McGraw-Hill, New York, 2002.

[5] Richards, M.A., *Fundamentals of Radar Signal Processing*, McGraw-Hill, New York, 2005.

[6] Swerling, P., "Radar Probability of Detection for Some Additional Fluctuating Target Cases," *IEEE Transactions on Aerospace and Electronic Systems,* vol. AES-33(2), pp. 698–708, April 1997.

[7] Weinstock, W., "Target Cross Section Models for Radar Systems Analysis," Ph.D. dissertation, University of Pennsylvania, 1964.

[8] Ray, H., "Improving Radar Range and Angle Detection with Frequency Agility," *Microwave Journal,* vol. 9, pp. 63–68, May 1966.

[9] Birkmeier, W.P., and Wallace, N.D., *AIEE Transactions on Communication Electronics*, vol. 81, pp. 571–575, January 1963.

[10] DiFranco, J.V., and Rubin, W.L., *Radar Detection*, Artech House, Dedham, MA, 1980.

[11] Shnidman, D.A., "Radar Detection Probabilities and Their Calculation," *IEEE Transactions on Aerospace and Electronic Systems*, vol. AES-31, no. 3, pp. 928–950, July 1995.

[12] Shnidman, D.A., "Update on Radar Detection Probabilities and Their Calculation," *IEEE Transactions on Aerospace and Electronic Systems*, vol. AES-44, no. 1, pp. 380–383, January 2008.

[13] Shnidman, D.A., "Calculation of Probability of Detection for Log-Normal Target Fluctuations," *IEEE Transactions on Aerospace and Electronic Systems*, vol. AES-27, no. 1, pp. 172–174, January 1991.

[14] Shnidman, D.A., "Expanded Swerling Target Models," *IEEE Transactions on Aerospace and Electronic Systems*, vol. AES-39, no. 3, pp. 1059–1068, July 2003.

[15] Nathanson, F.E., *Radar Design Principles*, 2d ed., McGraw-Hill, New York, 1991.

[16] Skonik, M. I., *Introduction to Radar Systems*, 3d ed., McGraw-Hill, New York, 2001.

[17] Edde, B., *Radar*: *Principles, Technology, Applications*, Prentice-Hall, Upper Saddle River, NJ, 1995.

[18] Levanon, N., *Radar Principles, Wiley Interscience*, New York, 1988.

[19] Mahafza, B. R., *Radar Systems Analysis and Design Using MATLAB*, Chapman & Hall/CRC, Boca Raton, FL, 2000.

7.9 PROBLEMS

1. Consider a conducting sphere with a radius a_s of 1 m. What is the RCS of this sphere at an RF of 10 GHz? Give the answer in units of both square meters and dBsm. (Assume the sphere is "much larger than" the wavelength.) What must be the side length a_t of a trihedral so that it has the same RCS at 10 GHz? What is the ratio of the size of the sphere compared with that of the trihedral, a_s/a_t?

2. In terms of D/λ, what is the two-sided "mainlobe width" (angular interval between the first zero of the pattern to either side of the peak) of the dumbbell target RCS pattern of Figure 7-5 in the vicinity of a nominal aspect angle of $\theta = 0^\circ$? Repeat for $\theta = 90^\circ$. Assume D/λ is an integer.

3. For a given integer value of D/λ, how many RCS peaks will occur in a compass plot such as Figure 7-6? Verify your answer for the case of $D/\lambda = 5$ by counting the lobes in the figure.

4. Suppose a stationary radar illuminates a complex, but stationary, target with a series of pulses. Which probability density function is an appropriate choice to represent the series of echo power measurements? Why?

5. The fourth-degree chi-square PDF used to model the case of one dominant scatterer with many small scatterers is an approximation to the exact model for this case, which is the Rician PDF. The Rician PDF has a variance of $\bar{\sigma}^2(1 + 2a^2)/(1 + a^2)^2$, where a^2 is the ratio of the RCS of the large scatterer to the combined RCS of the small scatterers. Show that when they both have the same mean $\bar{\sigma}$, their variances will also be the same if the Rician parameter $a^2 = 1 + \sqrt{2}$.

6. Suppose that a target was modeled as consisting of one large scatterer and many small ones but that the ratio a^2 of the large scatterer RCS to the sum of the small scatterer radar cross sections is 1 (instead of $1 + \sqrt{2}$ as assumed by the fourth-degree chi-square model). Assuming the means of the two distributions are the same, what degree $2m$ should be chosen for the chi-square so as to match the variance of the Rician (see Table 7-1)? Repeat for $a^2 = 10$. Note: m does not have to be an integer.

7. Part of the significance of choosing the probability density function used to model target RCS (or clutter or other interference) is that the differences in the "tails" of the PDF can have a significant impact on the probability of observing relatively large signal values, sometimes called signal "spikes." Recall that the probability that a random variable x described by a PDF $p_x(x)$ exceeds some value T is given by

$$\mathrm{P}\{x > T\} = \int_T^{+\infty} p_x(x)\, dx$$

Consider RCS data with a mean value (linear scale) of 1.0. Compute the probability that the RCS σ is greater than 2 when an exponential PDF is a good model for the RCS statistics and again when a fourth-degree chi-square is a good model for the statistics.

8. What is the maximum estimated decorrelation frequency step size Δf for a rectangular complex target like that shown in Figure 7-7 with $L_1 = L_2 = 3$ m when viewed by a radar operating at $f_0 = 5$ GHz? If $N = 10$ pulses are collected at frequencies f_0, $f_0 + \Delta f, \ldots, f_0 + (N-1)\Delta f$, what percentage of the nominal frequency, f_0, is the total change in frequency?

9. A rectangular target has dimensions $L_1 = 3$ m and $L_2 = 10$ m. What is the largest value of Δf required to decorrelate the RCS by frequency agility, regardless of aspect angle θ? At what aspect angle does this value occur?

10. The ASR-9 is a common airport surveillance radar in the United States. It has an RF of 2.8 GHz, 3 dB azimuth beamwidth θ_3 of 1.4°, and a rotation rate Ω of 12.5 revolutions per minute. Consider an aircraft at a range of 50 nmi (nautical miles). Assume the PRF is chosen to give an unambiguous range of 60 nmi. How many pulses will be transmitted during the time the aircraft is within the 3 dB mainlobe of the antenna on a single rotation? (This will be considered a single "scan" of the aircraft by the radar.)

11. Continuing problem 10, assume the aircraft is a Boeing 757 with a length of about 47 m and a wingspan of about 38 m, flying broadside to the radar at 120 knots. In the time the aircraft is in the mainbeam of the antenna on a single scan, what will be the change in the aspect angle, $\Delta\theta$, between the radar and aircraft? Based on this result, should pulse-to-pulse or scan-to-scan decorrelation be assumed for the pulse echoes received on a single scan?

12. Show that the gamma PDF of equation (7.11) reduces to the exponential PDF of equation (7.7) when $\alpha = 1$ and $\beta = \bar{\sigma}$ and to the fourth-degree chi-square of equation (7.9) when $\alpha = 2$ and $\beta = \bar{\sigma}/2$.